Preparation of Ion-exchanged Zeolite Nanoparticles by Laser Irradiation in Liquid and their Properties

Kishin Konishi and Hiroyuki Wada*

Tokyo Institute of Technology, 4259 Nagatsuta-cho, Midori-ku, Yokohama 226-8502, Japan
**Corresponding author's e-mail: wada.h.ac@m.titech.ac.jp*

Zeolite nanoparticles were prepared by laser irradiation of zeolites or ion-exchanged zeolites. Using ion-exchanged zeolite as a raw material, metal cations introduced into the pores caused local laser absorption, and zeolite nanoparticles were produced with a minimum size of 50 nm. X-ray diffraction and transmission electron microscopy images confirmed the crystal structure of the zeolite nanoparticles. It was found that the crystal structure was maintained up to the nanoparticles' surface. By changing the centrifugation intensity, nanoparticles of any size could be selectively recovered from dispersions containing nanoparticles with a wide size distribution. The volume zone of the obtained nanoparticles was estimated by comparing it with the calculated particle size value that all particles settled using Stokes' law.
DOI: 10.2961/jlmn.2024.02.2003
Keywords: zeolite, nanoparticles, laser, ion exchange, centrifugation

1. Introduction

Zeolites are porous aluminosilicates with a uniform pore size (about 1 nm) and ion exchange capacity. Various zeolite types with different pore sizes and compositions have been artificially synthesized for different purposes [1]. Synthesized zeolite is used, for example, as a deodorant [2] or adsorbent to remove emission control substances (such as NOx) contained in exhaust gas from factories and automobiles [3] and to remove impurities from various solvents in chemical plants [4]. It is also used as a catalyst for selective organic reactions using the molecular sieve effect of pores [5]. Furthermore, studies have been made in recent years to develop further physical properties by modifying the zeolite surface [6] and synthesizing metal nanoparticles inside [7].

Nanometer-sized zeolites are attracting attention because of their high specific surface area, and shortening the diffusion path into pores, which improves the accessibility of guest molecules into pores and improves dispersibility in solvents [8]. Several major zeolite nanoparticles have been synthesized by a bottom-up method [9-11]. However, the synthesis conditions must be a dilute solution, and the heating temperature and time must be appropriately controlled to suppress the zeolite crystal growth as much as possible. Moreover, a method of synthesizing by adding an organic template, such as tetramethylammonium hydroxide, and a method of synthesizing from an inert medium, such as a gelling polymer, are known to promote nucleation [12-14]. However, these methods have problems in terms of high production costs and wastewater pollution. Although various kinds of zeolites have been developed currently, the synthesis conditions of each one are different. However, it is more difficult to synthesize various kinds of zeolite nanoparticles.

A top-down approach using laser ablation in liquid is one of the promising methods to obtain nanoparticles by dispersing a target substance in a liquid and irradiating it with a pulsed laser. Various functional nanoparticles were prepared by laser processing [15-18]. It would be possible to obtain various types of zeolite nanoparticles such as A, X, Y, and so on by using commercially available zeolite as a raw material for laser ablation in liquid. Various types of zeolite nanoparticles can be easily produced in a short time and one step. In addition, it is possible to prevent the pores from being clogged by an excessively added organic substance since the nanoparticle-dispersed solution does not contain other organic substances. In the past, nanoparticle production by laser irradiation has been widely performed in producing metal or metal oxide nanoparticles. A high-temperature and high-pressure field are generated by focused irradiation of a solid target, and nanoparticles are produced through melting and plasma formation [19-21]. In contrast, preparing zeolite nanoparticles with complex metastable structures remains challenging. William T Nichols et al [22]. irradiated powdered LTA zeolite with a focused laser and reported that the size and crystallinity of the nanoparticles produced varied with the difference in laser power. As the power of laser irradiation was increased, the particle size could be reduced, but at the same time, zeolite nanoparticles with low crystallinity were produced. This indicates that if the laser power is too high, the metastable structure will be damaged by forming high-temperature plasma. In their research, the remaining issue was increasing energy absorption and fragment while avoiding melting and plasma formation due to laser irradiation.

In this study, ion-exchanged zeolites were used. Metal cations were introduced into the zeolite pores by performing ion exchange on the raw material zeolite. By inducing local laser light absorption into the introduced metal cations, zeolite was fragmented by using unfocused laser light. Top-down approaches are often challenged with maintaining surface crystallinity. The size and crystallinity of the prepared nanoparticles were investigated. By centrifuging zeolite nanoparticles with a wide size distribution, nanoparticles with the desired size were selectively recovered. At that time, the volume zone of the particle size of the produced zeolite nanoparticles was estimated by comparing it with the particle

size derived from the Stokes' equation, which all sedimented when the centrifugation conditions were changed.

2. Experimental

HSZ-320-HOA (SiO_2/Al_2O_3) = 5.6, Na_2O 4.0 wt%) was purchased from Tosoh Corporation as the raw material zeolite. The raw material was washed with ultrapure water 10 times (ultrasonic dispersion in ultrapure water followed by centrifugation at 500 rpm for 20 minutes to recover the precipitate). As a procedure for ion exchange, after dispersing the starting zeolite in ultrapure water, $CuCl_2$, $AgNO_3$, and $FeSO_4$ were added so that the supported metal cation amount was 1 wt%, and the mixture was stirred for 2 days. The resulting zeolite was dried in an oven at 120°C for 3 hours and stored as a powder sample. Diffuse reflectance ultraviolet-visible absorption spectra of raw material zeolites and ion-exchanged zeolites were measured using a spectrophotometer (DR UV–vis, JASCO, V-670).

0.02 g of a powdered zeolite sample was added to 20 mL of ultrapure water and dispersed using ultrasonic waves. The dispersion was irradiated with a nonfocused Nd:YAG laser (Spectron Laser system, SL8585G, SHG, wavelength of 532 nm, pulse duration of 13 ns, repetition frequency of 10 Hz) for 30 minutes. The irradiation area was measured in each experiment, and the laser power was adjusted so that the fluence was 3000 mJ/cm^2. Centrifugation was performed for 20 minutes while changing the rotation speed (500, 1000, 2000, 3000 rpm) because the raw material zeolite and nanoparticles were mixed in the dispersion after laser irradiation. 3 μL of the nanoparticle dispersion was dropped onto the elastic carbon support film on the copper grid and observed with a scanning electron microscopy (SEM, Hitachi High-technologies, S-4800, acceleration voltage of 5 kV, working distance of 8 mm). The secondary particle size (particle size in the aggregated state) of the dispersion was measured using dynamic light scattering (DLS, Sysmex, Zetasizer Nano, laser wavelength of 633 nm, and detection angle of 173°). The crystal structures of the powdered raw zeolite, Fe^{3+}-zeolite, and the obtained Fe^{3+}-zeolite nanoparticles were analyzed using X-ray diffraction method (XRD, Rigaku, Mini Flex 600, Cu-Kα radiation (λ_0 = 0.15418 nm), scan range of 5.0000–100.0000 deg.). Since the nanoparticles' yield was extremely small, the nanoparticle dispersions obtained in 10 experiments under the same conditions were combined and dried at 120°C to obtain a powder sample for measurement. Furthermore, for samples containing Fe^{3+}, it was necessary to measure them in the fluorescent X-ray reduction mode to suppress the background increase, which is a problem when measuring iron-based samples with a Cu-ray source. Accordingly, the scan speed was changed for the raw material zeolite powder and the others (scan speed at raw material zeolite: 2.0000 deg./min, at Fe^{3+}-zeolite and Fe^{3+}-zeolite nanoparticle: 1.0000 deg./min). Therefore, instead of simply comparing the intensities, we normalized the three samples and evaluated the changes in the crystal structure based on the peak positions and intensity ratios. The crystallite sizes of the three samples were calculated from the Full Width at Half Maximum (FWHM) at the first peak ($2\theta = 23.8°$) using the following Scherrer's equation.

$$D = \frac{K\lambda_0}{B\cos\theta} \quad (1)$$

where, D is the crystallite size, K=1.0747 is the Scherrer constant when the crystallite is assumed to be a sphere, and B is the FWHM. Furthermore, the field-emission transmission electron microscopy (FE-TEM, JEM-2100F, JEOL, acceleration voltage 200 kV) was used to evaluate the nanoparticles' crystallinity of about 50 nm. Moreover, elemental mapping was performed by transmission scanning electron microscopy–energy dispersive X-ray spectroscopy (STEM–EDS, JED-2300T) to investigate the composition.

3. Results and discussion

SEM images are shown for samples irradiated with a laser at varying fluences to zeolite that had not been ion-exchanged (Fig. 1). It was observed that the particles were finer than the raw material zeolite, and the particle size was about 200 nm to 500 nm regardless of the fluence. A possible zeolite fragmentation mechanism is energy storage through local absorption. Zeolite is a material with a large bandgap, and most of the laser light incident on the raw material zeolite is thought to pass through without being absorbed. Furthermore, laser ablation occurs by two-photon absorption, and as will be shown later in Figure 2, non-doped zeolite has no absorption at 266 nm. Therefore, laser ablation by two-photon absorption rarely occurred. However, a study by Nichols et al [22]. pointed out the possibility that crystal defects produced during zeolite synthesis and impurity metal cations, such as iron ions that are unintentionally incorporated, may lead to local energy storage by absorbing light. No significant change was observed due to fluence in the range of this experiment, and it was thought that further fragmentation and higher yield would be difficult in the laser irradiation of raw material zeolite. The local absorption points were increased by introducing metal cations into the pores by performing ion exchange on the raw zeolite.

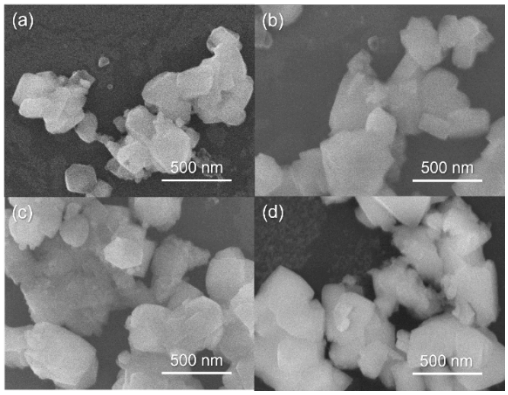

Fig. 1 SEM images of zeolite nanoparticles at each laser fluence: (a) 325 mJ/cm^2, (b) 750 mJ/cm^2, (c) 1500 mJ/cm^2, (d) 3000 mJ/cm^2.

Figure 2 shows the DR UV–vis spectra of ion-exchanged zeolites ion-exchanged with each metal cation. A change in the absorption spectrum shape and an absorbance increase were observed in the ion-exchanged zeolite compared to the raw material zeolite. Fe^{3+}-zeolite showed a broad absorption band from 200 to 400 nm. Peaks near 200 and 280 nm are assigned to isolated Fe^{3+} with tetrahedral and octahedral coordination, respectively [23-24]. The 300–400 nm absorption band was derived from oligonuclear $Fe^{3+}{}_xO_y$ clusters inside the zeolite [25]. For Cu^{2+}-zeolite, a strong peak was observed near 200 to 250 nm. This peak originated from the

$Cu^{2+} \leftarrow O^{2-}$ charge transfer transition due to the coordination bond of the ion-exchanged Cu^{2+} with the surrounding oxygen atoms [26]. Regarding Ag+-zeolite, although there was no significant absorbance increase, peaks were observed near 240 and 280 nm, which are considered to be Ag^{+}-derived peaks [27]. On the other hand, none of the ion-exchanged zeolites had an absorption band at the laser wavelength of 532 nm. All metal cations in the zeolite would not directly absorb the laser light irradiated at 532 nm this time. The absorption at 266 nm showed a large difference between non-doped zeolite and metal ion-doped zeolite. Through the absorption at 266 nm observed only in doped zeolites, laser ablation due to two-photon absorption occurred only in doped zeolites. In non-doped zeolite, there was no absorption at 266 nm and laser ablation due to two-photon absorption did not occur.

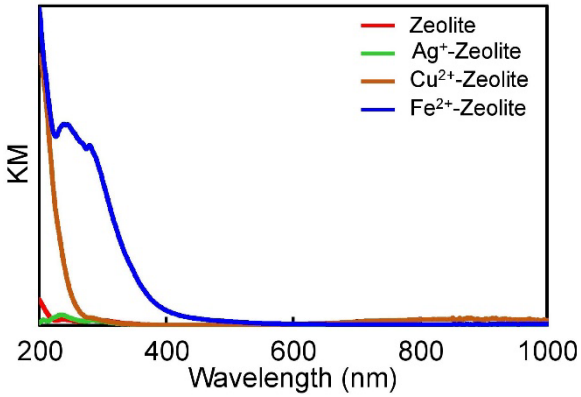

Fig. 2 Diffuse reflectance UV-vis spectrum for each ion-exchanged zeolite.

Figure 3 shows the SEM image of the sample irradiated with laser for each ion-exchanged zeolite. Fe^{3+}-zeolite (b), Cu^{2+}-zeolite (c), and Ag^{+}-zeolite (d) laser-irradiated samples showed smaller zeolite nanoparticles than the laser-irradiated samples of raw material zeolite (a). This suggests that the intentional metal cation introduction by ion exchange was effective for efficient fragmentation. On the other hand, however, the yield was extremely low and was below the detection limit of the electronic balance, so a quantitative increase in yield could not be confirmed. Considering the results in conjunction with the results in Fig. 2, multiphoton laser light absorption by metal cations or ion exchange of some metal cations to special positions is thought to be the cause of further fragmentation despite the absorption band increase, which is not at the laser wavelength. First, about the multiphoton laser light absorption, a bandgap that cannot be overcome with the energy of a single photon can be excited by irradiating a high-fluence laser light with the energy of multiple photons [28]. Since this study used 532 nm laser light, it is possible that the energy of the two photons could cause the excitation of an energy band corresponding to half the wavelength. It is necessary to use a laser light source with a small pulse width that is more likely to induce multiphoton absorption to expect a higher yield in the future. Alternatively, it may be necessary to introduce metal cations into more unstable positions by changing the amount or method of ion exchange. Rapid heat transfer occurs from metal cations that absorb energy locally within the pores to the surrounding lattice through electron-phonon coupling. As a result of the stress accumulated in the crystal lattice due to the lattice vibration, it was presumed that the bond breakage occurred and led to the miniaturization.

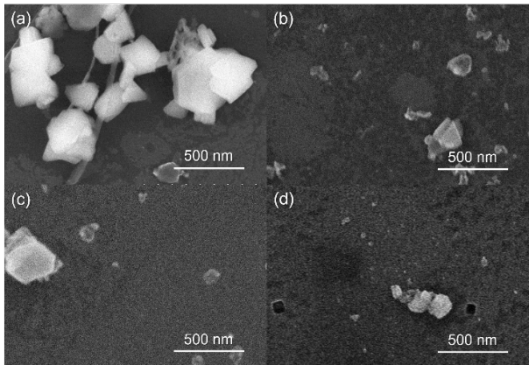

Fig. 3 SEM images of each ion-exchanged zeolite: (a) Zeolite, (b) Fe^{3+}-Zeolite, (c) Cu^{2+}-Zeolite, (d) Ag^{+}-Zeolite.

Figure 4 shows the XRD measurement results of the entire Fe^{3+}-zeolite nanoparticles obtained. These three data were normalized. All the peaks seen in the graph are attributed to Y-type zeolite (space group 227: Fd-3m, crystal phase name Sodium Aluminum Silicon Oxide). It was confirmed that there was no change in peak positions and intensity ratios in the three samples. It is known that the crystalline structure of zeolites does not change before and after ion exchange in small, well-dispersed quantities [29]. So, it can be inferred that Fe^{3+} was also sufficiently dispersed in this experiment. In addition, no change in peak position or intensity ratio was observed after laser irradiation, and no increase in baseline due to amorphous scattering was confirmed. This suggests that the crystallinity of the nanoparticles was maintained after laser irradiation. When the crystallite size was calculated using Scherrer's equation at 2θ = 23.8°, which is the first peak, for the raw material zeolite, it was 71.2 nm, for the Fe^{3+}-zeolite was 73.4 nm, and for the Fe^{3+}-zeolite nanoparticles were 69.5 nm. A slight decrease was observed after laser irradiation, but there was almost no change in the three samples. It can be inferred that fragmentation by laser irradiation does not cause significant damage to the crystallites themselves. In this study, it was not possible to experiment on the crystallite size effect of the starting zeolite. However, the small crystallite size of the raw material zeolite may be advantageous in producing nanoparticles by laser irradiation from the viewpoint of easily inducing fractures at crystal interfaces.

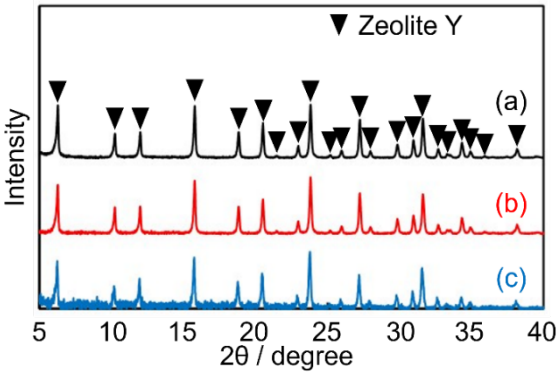

Fig. 4 XRD patterns of the products: (a) Raw material zeolite, (b) Fe^{3+}-Zeolite, (c) Fe^{3+}-Zeolite nanoparticles.

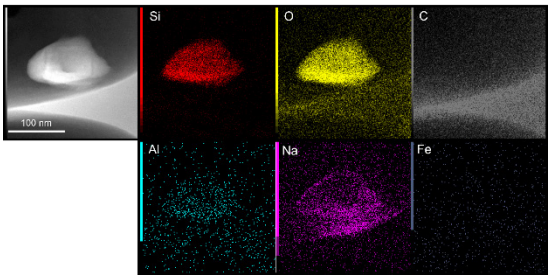

Fig. 5 STEM images and EDS elemental mapping of Fe^{3+}-Zeolite nanoparticles.

Figure 5 shows the STEM–EDS elemental mapping of the obtaine d small Fe^{3+}-zeolite nanoparticles. The nanoparticles confirmed in the STEM image were composed of zeolite constituent elements Si, O, Al, and Na, and it was verified that the obtained fine nanoparticles were zeolite nanoparticles. On the other hand, ion-exchanged Fe was hardly mapped. In this study, the supported metal cation amount was not large, and the metal cations dispersed in the fine nanoparticles may be difficult to detect by EDS. Since Fe was not detected in this study, it can be inferred that the iron ions dispersed in the zeolite did not change into aggregates such as FeO within the pores after laser irradiation.

TEM images of small Fe^{3+}-zeolite nanoparticles are shown in Figs. 6(a) and (b). Lattice fringes were also observed at the edges of the nanoparticles in the TEM images. This indicates that the Fe^{3+}-zeolite nanoparticles refined by local absorption by the laser retained their crystallinity on the crystal surface. Zeolite is a material exhibiting its function by introducing molecules into its pores [30,31] or that has excellent adsorption properties in its pores [32,33]. The nanoparticle surface crystallinity is very important in terms of pore accessibility [34]. FFT power spectra of the obtained TEM images were observed. Three strong points were confirmed in the spectrum of (c). Since points A and B are at the same distance from the center point, it was confirmed that lattice fringes spread in different directions with the same plane spacing in (a). Point C exists in the same direction as point B and at a different distance from the center. In the spectrum of (d), ring-shaped weak points were found here and there, indicating that the nanoparticles had a polycrystalline structure. It was suggested that fragmentation due to laser irradiation was not biased toward a specific crystal plane because there was no bias toward a specific plane through the two patterns. If melting nanoparticles occurred, crystallinity would be decreased, and amorphous would be created. However, the observation of the lattice fringes in Figs. 6(a) and (b) and points at the FFT power spectrum in Fig. 6(c) would imply the retention of crystallinity and the existence of pores of zeolite.

Figure 7 shows SEM images of the samples with different centrifugal strengths for the Fe^{3+}-zeolite nanoparticle dispersion. It was observed that only smaller particles remained as the revolution number increased. As for the shape, it was observed that the smaller particles had more anisotropy. Those with an irregular surface structure have a larger specific surface area than spherical particles. This change in shape was thought to be desirable when considering the application to catalytic reactions, in which the accessibility of guest molecules to pores is important.

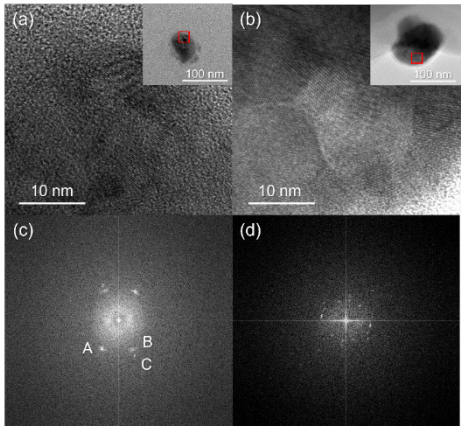

Fig. 6 (a) (b) TEM images of Fe^{3+}-Zeolite nanoparticles. (c) FFT pattern of (a). (d) FFT pattern of (b).

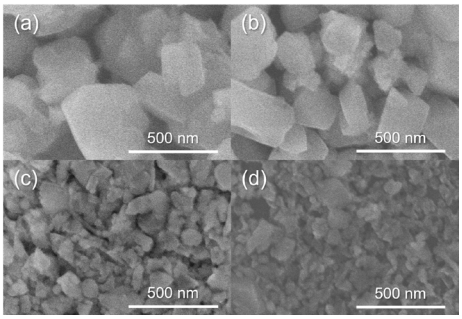

Fig. 7 SEM images of Fe^{3+}-Zeolite nanoparticles at each centrifugation speed: (a) 500 rpm, (b) 1000 rpm, (c) 2000 rpm, (d) 3000 rpm.

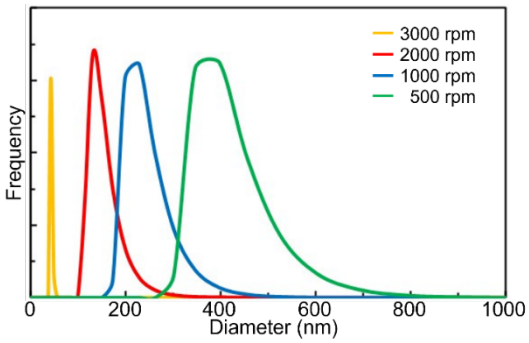

Fig. 8 DLS frequency distribution of secondary particle size of Fe^{3+}-Zeolite nanoparticles at each centrifugation speed.

Figure 8 shows the secondary particle size distribution by DLS. As for the secondary particle size, it was observed that only the smaller particle size remained by increasing the revolution number in the same manner as the primary particle size. As for the secondary particle size, it was observed that only the smaller particle size remained by increasing the revolution number in the same manner as the primary particle size. From these, zeolite nanoparticles of any particle size can be selectively recovered by changing the rotation speed during centrifugation. By combining laser irradiation and centrifugation, we easily prepared nanoparticles of the optimum size according to the purpose. In addition, since the primary particle size analyzed from the SEM image and the secondary particle size measured by DLS were almost the

same, it was found that the nanoparticles were not aggregated in the supernatant liquid and were in a dispersed state.

Figure 9 shows the primary particle size distribution as measured by SEM and the particle size that was completely precipitated, which was derived from the Stokes equation. The calculation was performed according to the following procedure. First, the sedimentation velocity of spherical nanoparticles in a stationary solution can be expressed by the following equation according to Stokes' law.

$$v = \sqrt{\frac{4(P_s - P_w)gd}{3P_w C_d}} \quad (2)$$

where, P_s is particle density (kg/m^3), P_w is dispersion medium density (kg/m^3), g is the gravitational acceleration (9.81 m/s^2), d is particle size (m), and C_d is the drag coefficient. The drag coefficient can be approximated by the following formula when the particles settle quietly without disturbing the dispersion medium.

$$C_d = \frac{24}{Re^*} \quad (3)$$

where Re^* is the particle Reynolds number, expressed by the following equation.

$$Re^* = \frac{vd}{\eta / P_w} \quad (4)$$

where η is the viscosity (Pa·s) of the dispersion medium. During centrifugation, nanoparticles can be expressed as follows using the rotation radius r (m) and the rotation angular velocity ω proportional to the rotation speed N instead of the gravitational acceleration g [35].

$$v = \frac{(P_s - P_w)d^2}{18\eta} \times r\omega^2 \quad (5)$$

and

$$\omega = 2\pi \frac{N}{60} \quad (6)$$

During centrifugation, the particle velocity v can be expressed as the change in the radius of gyration with respect to time, so it is dr/dt. From here, the sedimentation time T (s) can be expressed as follows by performing integration from $R_{min} \rightarrow R_{max}$ (liquid surface → centrifugal tube bottom) with the radius of gyration as a variable [36].

$$T = \frac{18\eta(\ln R_{max} - \ln R_{min})}{(P_s - P_w)d^2\omega^2} \quad (7)$$

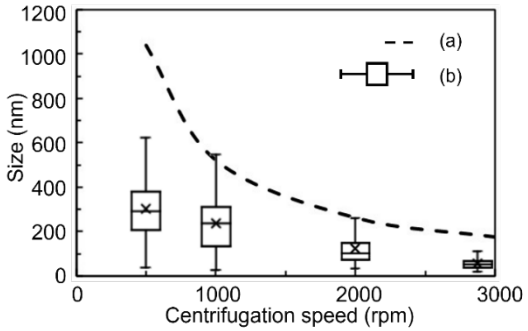

Fig. 9 Relationship between centrifugal speed and particle size: (a) Maximum fully precipitated particle size (calculated value), (b) Primary particle size distribution (SEM).

This sedimentation time varies depending on the particle size of the nanoparticles and the centrifugation speed. In this study, centrifugation was carried out for 20 minutes, so we calculated the particle size that would sediment in just 20 minutes at each rotation speed and compared it.

The primary particle size distribution was below the calculated fully precipitated particle size. It showed that the theoretical calculation using Stokes' law which assumes spherical nanoparticles, can be applied to separating anisotropic zeolite nanoparticles fragmented by laser irradiation. As the centrifugation rotation speed decreased, a larger divergence was observed between the total sedimentation particle size and the particle size. It is considered that this is because few nanoparticles were produced by laser irradiation in the dissociated particle size range. This suggests that the volume zone of nanoparticles produced by laser irradiation in this study was about 300 ~ 400 nm.

4. Conclusions

In this study, nanoparticles were produced by unfocused irradiation of a commercially available zeolite with a nanosecond laser with a wavelength of 532 nm. It was speculated that the refinement was caused by local energy accumulation due to impurity metal cations and crystal defects in the raw material zeolite. In addition, the fragmentation progressed by introducing metal cations such as Fe^{3+} into the pores. The diffuse reflectance UV–vis spectrum of the ion-exchanged zeolite showed no absorbance increase at 532 nm. This suggests that multiphoton excitation by laser light and the metal cation arrangement at irregular positions may greatly affect fragmentation. It is necessary to devise ways to efficiently induce these absorptions to improve the yield in future research. It was confirmed by XRD measurement that the crystal structure did not change in all three samples, raw zeolite, ion-exchanged zeolite, and laser-irradiated zeolite nanoparticles. Crystallite size calculation using Scherrer's equation suggested that zeolite produced for industrial use has a small crystallite size, which may work favorably in the production of nanoparticles by laser irradiation. Lattice fringes in the TEM image revealed that the crystal structure was maintained up to the surface of the zeolite nanoparticles. This shows great potential for surface damage, which has been viewed as a problem in previous top-down approaches. By using centrifugal separation, zeolite nanoparticles with a wide size distribution were selectively recovered. Comparison with the sedimentation particle size obtained from Stokes' law suggested that many nanoparticles with a particle size of about 400 nm were produced by laser irradiation.

Acknowledgments

The authors wish to thank M. Hara, Y. Kitamoto and K. Nakamura at Tokyo Tech for laser process and measurements. This study was supported by the Collaborative Research Project of Materials & Structures Laboratory (Tokyo Tech.) and Suzukakedai Materials Analysis Division (Tokyo Tech.).

References

[1] C. Baerlocher, L.B. McCusker, and D.H. Olson: “Atlas of Zeolite Framework Types” ed. by W.M. Meier (Elsevier, Amsterdam, 2007).

[2] I. Masakado and M. Akihiro: JP Patent 2002248317 A (2001).

[3] L. Yuejin and W. K. Hall: J. Phys. Chem., 94, (1990) 6145.
[4] D. Thomas: Top. Catal., 13, (2000) 349.
[5] M. Koji, H. Yuichiro, O. Kaito, U. Yoshiaki, T. Shunsuke, and N. Norikazu: J. Catal., 342, (2016) 63.
[6] N.M. Mahmoodi and M.H.S. Dastgerdi, Microchem. J., 145, (2019) 74.
[7] P.W. Andrey, F. Davide, K. Oliver, and B.A. Jeroen: ACS. Catal., 9, (2019) 2303.
[8] T. Lubomira, V.P. Valentin, Nanozeolites: Chem. Mater., 17, (2005) 2494.
[9] I. Lama, B.N. Krassimir, C. Guillaume, D. Luc, and V. Valentin: Chem. A. Eur. J., 17, (2011) 2199.
[10] W. Toru, I. Akio, I. Satoshi, T. Junichi, S. Kaku, K. Katsutoshi, M. Takeshi, K. Yoshihiro, and N. Atsushi: Cryst. Growth. Des., 11, (2011) 5153.
[11] L. Qinghua, M. Boriana, C. Derek, and S. Johan: Micropor. Mesopor. Mater., 43, (2001) 51.
[12] H. Limin, W. Zhengbao, S. Jinyu, M. Lei, L. Quanzhi, Y. Yushan, and Z. Dongyuan: J. Am. Chem. Soc., 122, (2000) 3530.
[13] W. Huanting, H. A. Brett, and Y. Yushan: J. Am. Chem. Soc., 125, (2003) 9928.
[14] M. Svetlana, O. H. Norman, V. Valentin, and B. Thomas: Sci., 283, (1999) 958.
[15] Haibo Zeng,Xi-Wen Du,Subhash C. Singh, Sergei A. Kulinich, Shikuan Yang, Jianping He, and Weiping Cai: Adv. Func. Mater., 22, (2012) 1333.
[16] Dongshi Zhang, Bilal Goekce, and Stephan Barcikowski: Chem. Rev., 117, (2017) 3990.
[17] Yaohui Zhan, Lei Zhang, Mohsen Rahmani, Vincenzo Giannini, Andrey E. Miroshnichenko, Minghui Hong, Xiaofeng Li, Stefan A. Maier, and Dangyuan Lei, ACS Photonics, 8, (2021) 166.
[18] Lianwei Chen, and Minghui Hong: Opto-Electr. Sci., 1 (2022) 210007.
[19] T. Takeshi, I. Kenzo, W. Norihisa, and T. Masaharu: Appl. Surf. Sci., 202, (2002) 80.
[20] T. Yoshihiro and M. Fumitaka: Chem. Phys. Lett., 599, (2014) 110.
[21] J. Jin-Woo, Y. Sangwoo, C.W. Hae, K. Joohan, F. Dave, and C. Sung-Hak: Appl. Sci., 8, (2018) 112.
[22] N. T, William, K. Tetsuya, S. Yukichi, S. Yoshiki, S. Takeshi, and K. Naoto: J. Phys. Chem. B, 110, (2006) 83.
[23] M. S. Kumar, M. Schwidder, W. Grünert, and A. Brückner: J. Catal., 227, (2004) 384.
[24] L. Čapek, V. Kreibich, J. Dědeček, T. Grygar, B. Wichterlová, Z. Sobalík, J.A. Martens, R. Brosius, and V. Tokarová: Micropor. Mesopor. Mater., 80, (2005) 279.
[25] P. Marturano, L. Drozdová, G.D. Pirngruber, A. Kogelbauer, and R. Prins: Phys. Chem. Chem. Phys., 3, (2001) 5585.
[26] A. Kharchenko, V. Zholobenko, A. Vicente, C. Fernandez, H. Vezin, V. D. Waele, and S. Mintova: Phys. Chem. Chem. Phys., 20, (2018) 2880.
[27] C. Shi, M. Cheng, Z. Qu, and X. Bao**:** J. Mol. Catal. A: Chem., 235, (2005) 35.
[28] K.P. Aicher, U. Wilhelm, and J. Grotemeyer: J. Am. Soc. Mass. Spectrom., 6, (1995) 1059.
[29] L. Li, Q. Shen, J. Li, Z. Hao, Z.P. Xu, and G.Q.M. Lu: Appl. Catal. A. Gen., 344, (2008) 131.
[30] M. Pauchard, A. Devaux, and G. Calzaferri: Chem. Eur. J., 6, (2000) 3456.
[31] G. Calzaferri, D. Brühwiler, S. Megelski, M. Pfenniger, M. Pauchard, B. Hennessy, H. Maas, A. Devaux, and U. Graf: Solid State. Sci., 2, (2000) 421.
[32] N. Patdhanagul, T. Srithanratana, K. Rangsriwatananon, and S. Hengrasmee: Micropor. Mesopor. Mater., 131, (2010) 97.
[33] O.O. Ltaief, S. Siffert, S. Fourmentin, and M. Benzina: Comptes Rendus Chimie, 18, (2015) 1123.
[34] Y. Hiroki, I. Takayuki, L. Zhendong, N. Yusuke, O. Koji, K. Shinji, O. Tatsuya, and W. Toru: Cryst. Growth. Des., 16, (2016) 3389.
[35] B.D. Hames: "Centrifugation: a practical approach" ed by D. Rickwood, (IRL Press, Oxford, 1984).
[36] T. Svedberg and J. B. Nichols: J. Am. Chem. Soc., 45, (1923) 2910.

(Received: March 19, 2023, Accepted: May 2, 2024)